Annual and semiannual VTEC effects at low solar activity based on GPS observations at different geomagnetic latitudes

M. P. Natali[1,2] and A. Meza[1,2]

[1]   The aim of this work is the analysis of the annual, semiannual, and seasonal effects in the total electron content (TEC) of the terrestrial atmosphere during low solar activity. Spatial and temporal ionospheric variability are investigated from global International Global Navigation Satellite System Service (IGS) VTEC maps during low solar activity in 2006. Two different techniques, principal component analysis (PCA) and Fourier analysis, are applied to the data set. Applying the PCA technique on a time series of global IGS VTEC maps gives us a method to analyze the main ionospheric anomalies on a global scale. The Fourier series provide us a comparison with the results obtained with PCA. The behavior of VTEC variations at 2 h periods centered at 1200 and 2200 local time (LT) are analyzed. Particular characteristics associated with each period and with the geomagnetic region are highlighted. All the stations show an annual behavior, which means that the maxima variations of the VTEC occur in summer while minimum variations are in winter, except in the stations located at the Northern Hemisphere at noon. Some regions show patterns of the semiannual anomaly during local noon, and it is also possible to see a higher peak of VTEC during spring rather than autumn in the Northern Hemisphere. However, if we analyze the pattern in the Southern Hemisphere, both peaks in equinox are of the same magnitude. Results obtained with Fourier series are comparable with the ones mentioned above.

1.   Introduction

[2]   *Chapman* [1931] developed a formula that describes the rate of production of ion-electron pairs as the product of four terms: the intensity of ionizing radiation at some level of the atmosphere, the concentration of atoms or molecules capable of being ionized by that radiation, the absorption cross section, and the ionization efficiency. Any departure from this "solar-controlled" behavior in the ionosphere is considered as anomaly. In fact, the F2 layer is anomalous rather than being simply described by the solar zenith angle as Chapman's theory predicts. There are many well-known anomalies in the F2 layer. Several authors have analyzed these variations and have identified three major components: winter maximum (seasonal), equinoctial maxima (semiannual), and a component that peaks in December to January (annual). Several explanations have been proposed for these phenomena. They can be grouped into three categories: geometrical, thermal, or chemical. Among the most accepted theories we can mention: *Torr and Torr* [1973] constructed global maps that represent the anomalies for different solar activity, and *Rishbeth and Setty* [1961] proposed that the winter or seasonal anomaly could be attributed to a seasonal change in chemical composition of the neutral air. Several authors have found different explanations to the semiannual anomaly, like variations in the solar wind [*Lal*, 1992, 1998] or an increase of the internal thermospheric mixing at solstice [*Fuller-Rowell*, 1998]. A possible cause of the annual anomaly is the changing Earth-Sun distance between June and December together with some associated atmospheric processes [*Buonsanto*, 1986].

[3]   In recent years, a database of ionospheric total electron content (TEC) derived from GPS observations produced by a worldwide network of continuously tracking stations has been used to investigate the local and regional characteristics of various anomalies [*Huang and Cheng*, 1996; *Wu et al.*, 2004]. The worldwide GPS network is managed by the International Global Navigation Satellite System Service (IGS).

[4]   In May 1998, IGS created the Ionosphere Working Group [*Feltens and Schaer*, 1998]. Of the scientific groups and institutes that are presently dedicated to ionospheric studies using GPS observations, three can be distinguished as the most important: the Center for Orbit Determination in Europe, which belongs to the Astronomical Institute of the University of Bern, Switzerland (http://www.aiub.unibe.ch/igs.html); the NASA Jet Propulsion Laboratory (JPL) (http://iono.jpl.nasa.gov), Pasadena, California; and the Astronomy

[1]Facultad de Ciencias Astronómicas y Geofísicas, Universidad Nacional de La Plata, La Plata, Argentina.
[2]Consejo Nacional de Investigaciones Científicas y Técnicas, Buenos Aires, Argentina.

and Geomatics group (gAGE) (http://gage1.upc.es), Barcelona, Spain. The global integration and modeling computed by each group is made available for the users as a file in the IONosphere map EXchange (IONEX) format [*Schaer et al.*, 1998]. The file contains all the information relative to the computation process and the VTEC information is presented in the form of a grid of 2.5° in latitude and 5° in longitude.

[5] The principal component analysis (PCA) method is regularly used by meteorologists and oceanographers as a tool for the analysis of the spatial or temporal variability of physical fields. PCA is the decomposition of a data set into a base of orthonormal functions that are directly determined by the data set itself. This mathematical procedure transforms a set of correlated variables into a number of uncorrelated variables called principal components. Several investigators have used the PCA technique to help isolate the cause of the sea level change signals [*Nerem et al.*, 1994, 1997]. It has also been used for empirical ionospheric modeling [*Zhao et al.*, 2005; *Meza and Natali*, 2008].

[6] In this paper, the annual, semiannual, and seasonal variations of the ionosphere during low solar activity throughout the year 2006 are analyzed using global IGS VTEC maps. Applying the PCA technique on a time series of IGS VTEC global maps gives us an efficient method to analyze the main ionospheric anomalies on a global scale. The behavior of VTEC variations at 2 h periods centered at 1200 and 2200 local time (LT) is analyzed. Particular characteristics associated with each period and with the geomagnetic region are highlighted.

[7] After a brief description of the data acquisition and method, the PCA and Fourier series are applied on the data set. Then the analysis of the results in the physical frame is described. Finally, the effects of the ionospheric anomaly trough IGS VTEC global maps are evaluated and discussed.

2. Methodology

2.1. Principal Component Analysis

[8] PCA is well suited for the analysis of multivariate time series. One main reason for that is that the technique can be used to identify spatial structures that have dominant contribution to the total variability together with their time evolution without the need to propose any particular a priori functional model.

[9] PCA is used to express a correlated data set on a new orthonormal base of minimum dimension. The shape of the base functions is determined from the data set itself. This method is of special interest when the phenomena under study are not necessarily a superposition of well-known simple components that would point other techniques (e.g., Fourier analysis) as more adequate. This method has been used in a variety of oceanographic and meteorological analyses to identify the principal modes of variability.

[10] In the next paragraph, a brief description of the algebraic essentials of PCA is presented. For further details about the algebraic foundations of PCA, see *Preisendorfer* [1988]. A description of the technique with focus on its application for TEC analysis is given by *Meza and Natali* [2008].

[11] Let $\mathbf{z}(t, x)$ be VTEC measures, at point x (latitude and longitude) in the atmosphere at time t. Let this measurements be taken over the set of locations $x = 1, \ldots, p$ at times

$t = 1, \ldots, n$. The first step in PCA is to center the time series on their time averages. This is:

$$\mathbf{z}'(t,x) = \mathbf{z}(t,x) - \overline{\mathbf{z}}(t,x) \qquad (1)$$

$$\text{with,} \qquad \overline{\mathbf{z}}(t,x) = \frac{\sum_{t=1}^{n} \mathbf{z}(t,x)}{n} \qquad (2)$$

[12] These collections can be thought as $p \times 1$ (i.e., column) vectors $\mathbf{z}'(t) = \{\mathbf{z}'(t, 1), \ldots, \mathbf{z}'(t, p)\}$ forming a swarm of points about the origin of a p-dimensional Euclidean space (E_p). Now it is possible to construct the symmetric scatter matrix in E_p:

$$\mathbf{S} = \sum_{t=1}^{n} \mathbf{z}'(t)\mathbf{z}'^{\mathrm{T}}(t) \qquad (3)$$

This matrix has a set of p orthonormal eigenvectors $\mathbf{e}_j = [\mathbf{e}_j(1), \ldots, \mathbf{e}_j(p)]^{\mathrm{T}}$, $j = 1, \ldots, p$. These are the empirical orthogonal functions: empirical because they arise from data, orthogonal because they are uncorrelated over space:

$$\begin{cases} \sum_{x=1}^{p} \mathbf{e}_j^{\mathrm{T}}(x)\mathbf{e}_k(x) = \begin{array}{l} 0 \quad \text{if} \quad j \neq k \\ 1 \quad \text{if} \quad j = k \end{array} \quad j,k = 1,\ldots,p \end{cases} \qquad (4)$$

From these $\mathbf{e}_j$ we can construct the principal components (or amplitudes) of the data set, $\mathbf{a}_j(t)$:

$$\mathbf{a}_j(t) = \sum_{x=1}^{p} \mathbf{z}'(t,x)\mathbf{e}_j(x) = \mathbf{z}'(t)^{\mathrm{T}}\mathbf{e}_j \qquad (\text{Analysis of } \mathbf{z}') \qquad (5)$$

where $t = 1, \ldots, n$; $j = 1, \ldots, p$. These $\mathbf{a}_j(t)$ can be thought of as a family of time series $\{\mathbf{a}_j(t): t = 1, \ldots, n\}$. The most important property of these time series is that they are mutually uncorrelated, carrying information about the variance of the data set along the directions $\mathbf{e}_j$:

$$\sum_{t=1}^{n} \begin{cases} \mathbf{a}_j^{\mathrm{T}}(t)\mathbf{a}_k(t) = \begin{array}{l} 0 \quad \text{if} \quad j \neq k \\ 1_j \quad \text{if} \quad j = k \end{array} \quad j,k = 1,\ldots,p \end{cases} \qquad (6)$$

where 1_j is the jth eigenvalue of $\mathbf{S}$. Finally, and most importantly, the original centered data set can be exactly represented in the form:

$$\mathbf{z}'\mathrm{T}(t,x) = \sum_{j=1}^{p} \mathbf{a}_j(t) = \mathbf{e}_j^{\mathrm{T}}(x) \qquad (\text{Synthesis of } \mathbf{z}') \qquad (7)$$

where $t = 1, \ldots, n$; $x = 1, \ldots, p$. By eigenvalue decomposition of the covariance matrix of TEC anomalies, the PCA technique identifies those spatial structures of the ionosphere variability that have dominant contribution to the total variance (given by the sum of all eigenvalues). The spatial structure of the ionosphere variability is represented by the eigenvector and its temporal evolution is described by a series of coefficients, called principal components. Eigenvector and principal components together are called mode. Modes are ordered according to decreasing eigen-
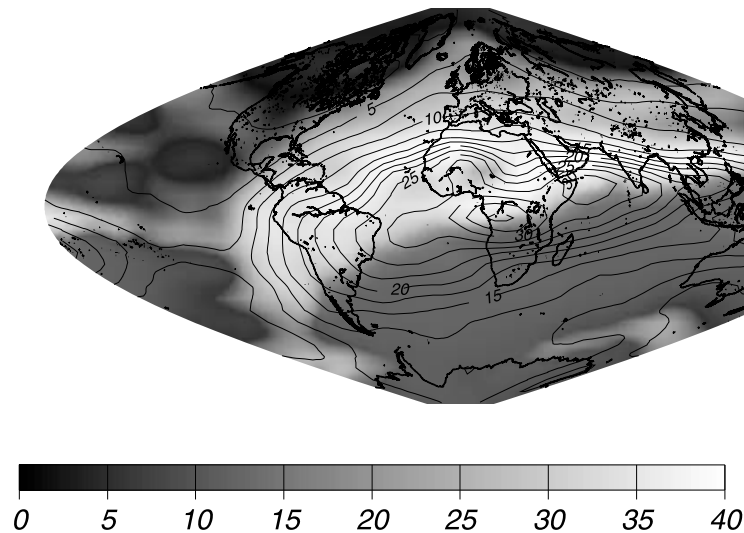
Figure 1. IGS VTEC global map for the day 350 at 1200 LT.

values, such that the first mode represents the largest part of the variance, the next mode the second largest part, etc.

[13] The PCA analysis software we wrote for this work was based on the subroutines "jabob" and "eigsrt" from *Press and Flannery* [1995]. In many cases, the scatter matrix **S** may become very large, so it is difficult to compute eigenvalues; an alternative is to use singular value decomposition over $\mathbf{z}'$.

2.2. Chosen Scenario

[14] The IONEX format allows the storage of snapshots of the electron density (including associated RMS information) referring to particular epochs and to a 2-D or even 3-D Earth-fixed grid. IONEX data supply a good estimation of the worldwide VTEC. These data provide VTEC values around the world at intervals of 2.5° in latitude and 5° in longitude (Figure 1).

[15] Global IGS VTEC maps during low solar activity (from January to December 2006) are used in this work.

These VTEC maps show a global snapshot of the ionosphere every 2 h. Therefore, the main geographical VTEC variation that can be seen on them is the ionization due to solar radiation. Since we are not interested in analyzing that effect but instead the ionospheric response to similar conditions on different locations, we reorganized the VTEC data as follows: Two different solar radiation conditions were selected for analysis from each daily global data set, composed by 12 VTEC maps. Two maps were constructed. One of them corresponded to 1200 LT worldwide; the other one corresponded to 2200 LT. The temporal series were constructed in the following way: Assuming that the ionosphere doesn't change in a 2 h window, we took 30° slices from all VTEC maps for each day, centered on the same local time. These slices were then merged into a new VTEC map according to their central longitude. This procedure resulted in two new VTEC maps per day, corresponding to 1200 LT and 2200 LT worldwide. The complete data set consists of two series of VTEC maps covering the year
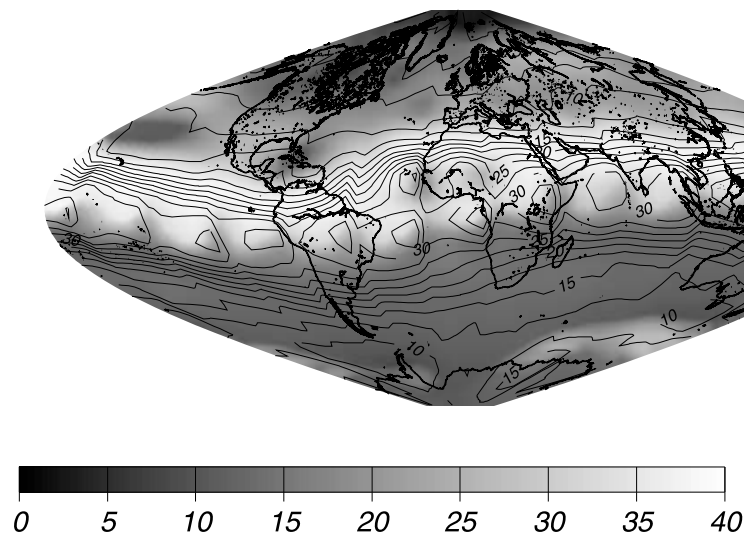
Figure 2. IGS VTEC map after the reorganization of the data. This is a snapshot of the ionosphere for 1200 LT for the day 350 of 2006.
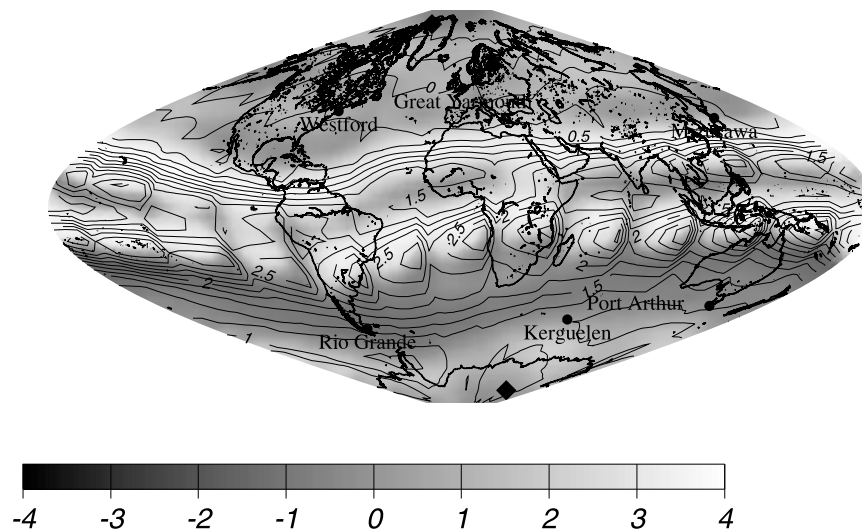
Figure 3. Spatial variation in the first mode for 1200 LT.

2006 for 1200 LT and 2200 LT, respectively. It is important to stress that there are no further processes applied to the data besides this sorting. No smoothing was applied in the process of building these map time series. An example of the resulting daily map for 1200 LT for the day 350 is shown in Figure 2. Once these VTEC grids were built for every day in 2006, PCA and Fourier analysis were applied to each of the time series obtained in order to estimate the eigenvalues and eigenvectors associated to each data set.

3. Results and Discussion

[16] The VTEC behaviors are analyzed during low solar activity at different local time centered in 1200 LT for noon and 2200 LT for the night.

3.1. PCA Analysis

[17] Figures 3 to 6 illustrate the spatial variation and Figures 7 to 10 show the time variation obtained for the first

and second mode using PCA on the global IGS VTEC maps at different local times. In all figures, the geomagnetic pole is represented by a diamond. In Figures 7 to 10, the x axis is represented the day of year and the y axis is the amplitude.

3.1.1. Local Time: Noon

[18] In Figure 7, showing the amplitude for mode 1 at noon, it is possible to see a main annual component modulated by a semiannual component. From carrying out Fourier analysis on this mode, we found an annual component modulated by a semiannual component that is 50% smaller than the annual one, with a 180° phase shift. Showing VTEC variations with maximal values between October and February and minimal in June and July. The maximum variations are distributed near the geomagnetic equator and at middle and high latitudes in the Southern Hemisphere. For mode 2, in Figure 8, it is possible to see a semiannual component modulated by an annual one. Doing the same Fourier analysis on this mode, an annual and semiannual component in phase and with similar amplitudes
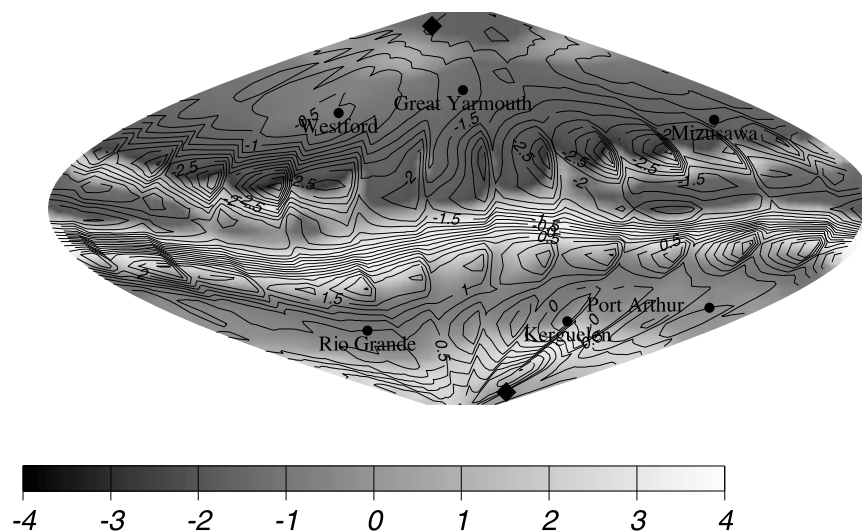

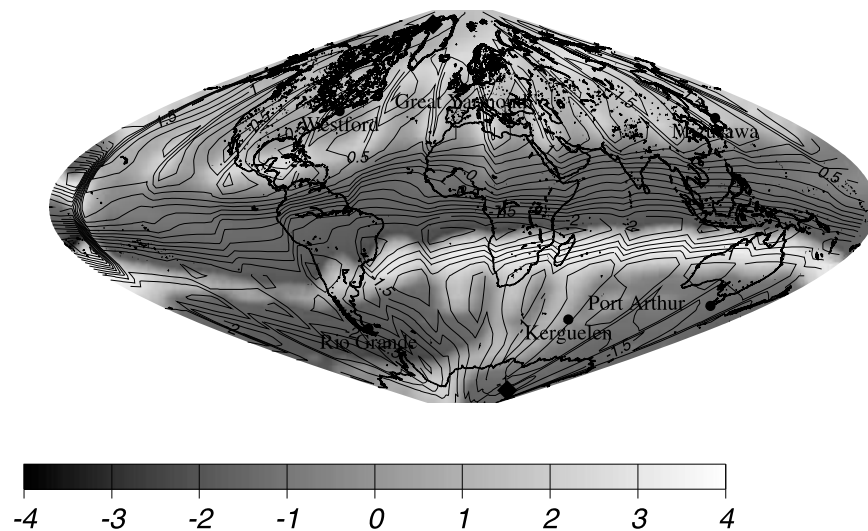**Figure 4.** Spatial variation in the second mode for 1200 LT.

Figure 5. Spatial variation in the first mode for 2200 LT.

was found. The maximum variations are distributed close to the geomagnetic equator and at middle latitudes in the Northern Hemisphere. The values are negative, so the amplitude (Figure 8) multiplied by its eigenvector shows maximum variability during the equinoxes, and results in a March–April equinox peak that is higher than the September–October one.

3.1.2. Local Time: Night

[19] In Figure 9, representing the amplitude for mode 1 at night, a purely annual component can be seen. The variations are lower than those obtained at noon, and they are positive in the Northern Hemisphere and negative in Southern Hemisphere. For mode 2, Figure 10, a semiannual component is modulated by an annual one, resulting in the March–April equinox peak being higher than the September–October one. Performing Fourier analysis on these two modes, similar results were found. The maximum variations are distributed close to equatorial region.

[20] To do the time analyses based on *Zou et al.* [2000], six stations at different latitude and longitude sectors were selected. We classify the stations by whether they are in near-geomagnetic pole longitudes, which are the North Atlantic (European/North American) sector in the Northern Hemisphere and the Australian sector in the Southern Hemisphere, or far from geomagnetic pole, which are the East Asian and South Atlantic sectors: (1) near geomagnetic pole, high midlatitudes: Great Yarmouth (52°N, 1°E), Kerguelen (49°S, 70°E); (2) near geomagnetic pole, lower midlatitudes: Port Arthur (43°S, 147°E), Westford (42°N, 72°W); (3) far from geomagnetic pole: Río Grande (53°S, 68°W), Mizusawa (39°N, 141°E).

[21] Figures 11 and 12 are compound, using the spatial variation (Figures 3 to 6) and the time variation (Figures 7 to 10), respectively. Figure 11 shows that for northern stations (Great Yarmouth, Westford, and Misuzawa) VTEC variability at midsummer and midwinter are nearly equal at
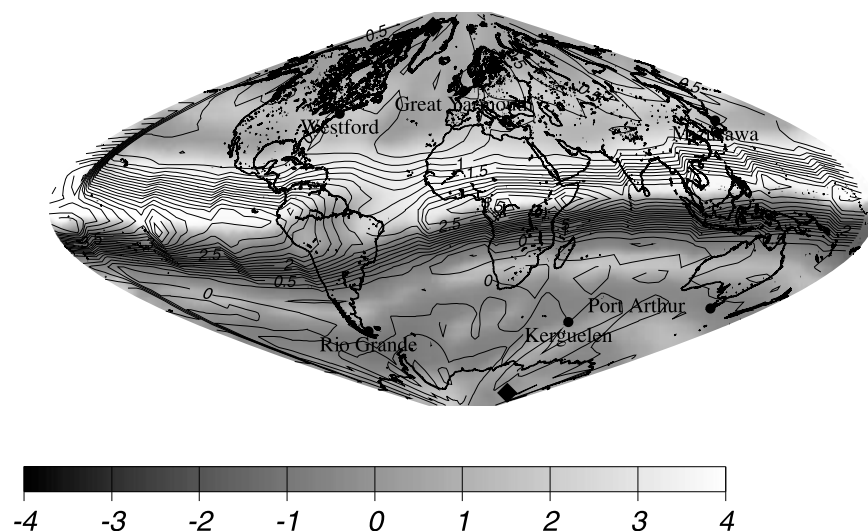

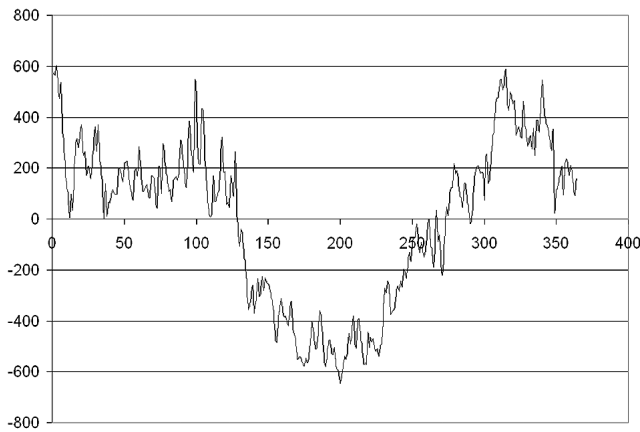**Figure 6.** Spatial variation in the second mode for 2200 LT.

Figure 7. Time variation in the first mode for 1200 LT.

Figure 9. Time variation in the first mode for 2200 LT.

noon. It is also possible to see patterns of the semiannual anomaly, which a higher amplitude in VTEC variations during spring than autumn. For southern stations at noon, it is possible to see principally an annual behavior of the VTEC variability (i.e., a maximum at summer) with secondary maximum at midequinox. This can be regarded as an effect of the annual anomaly, which opposes the seasonal anomaly in the Southern Hemisphere.

[22] Figure 12, for the night, shows that summer VTEC variability exceeds winter VTEC variability at all stations, so the annual behavior with summer peak can be seen independently of the geomagnetic region. It is possible to see a weak component of the semiannual anomaly in the Northern Hemisphere, particularly in Westford and Mizusawa, resulting in a rather flat maximum near March equinox.

[23] *Zhao et al.* [2007] used global ionospheric maps of TEC to study features of the annual and semiannual anomalies in the interval from 1999 to 2005. These TEC maps were, in turn, used to estimate the annual-to-mean amplitude ratio, A_1, and the semiannual-to-mean amplitude ratio, A_2, as well as the latitudinal symmetrical and asymmetrical parts, A' and A'' of A1, respectively. The author defines the symmetrical and asymmetrical indices as:

$$A' = (A_1(MLAT) - A_1(-MLAT))/2 \qquad (8)$$
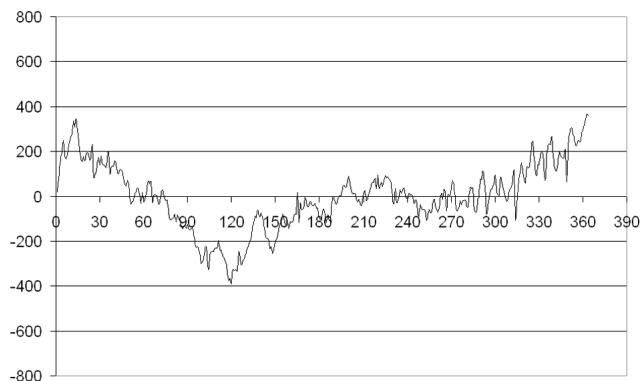
$$A'' = (A_1(MLAT) + A_1(-MLAT))/2 \qquad (9)$$

where

$$A_1 = TEC1/TEC0 \qquad (10)$$

where TEC1 is the annual component, TEC0 is the annual average value of TEC, and MLAT is the magnetic latitude. A' denotes the amplitude of the seasonal variation and A'' represents the annual anomaly.

[24] Figure 13 shows the symmetric and asymmetric distribution using equations (8) and (9) [*Zhao et al.*, 2007]. In our analysis, A1 is the average over longitudes for each magnetic latitude for mode 1 at 1200 LT and 2200 LT. After that, equations (8) and (9) were applied to this average, resulting the symmetric and asymmetric profiles (Figure 14). It should be noted that the initial phase for the 2200 LT occurs in June, while in the work of *Zhao et al.* [2007] the initial phase occurs in December, so a factor of –1 where applied in the figures.

[25] Looking at these profiles and considering the time variations of the amplitude for each mode, it is possible to see an annual variation for mode 1 at 1200 LT with the maximum in December–March and for 2200 LT in mode 1 with the maximum in the June–July months.

[26] In Figure 13, the noon anomaly at midlatitudes is absent [*Zhao et al.*, 2007], with A'' being negative. It is possible to see this behavior in Figure 14 (symmetric profile at 1200) where the profile is negative for all latitudes, and the seasonal anomaly is absent. For the asymmetric profile,
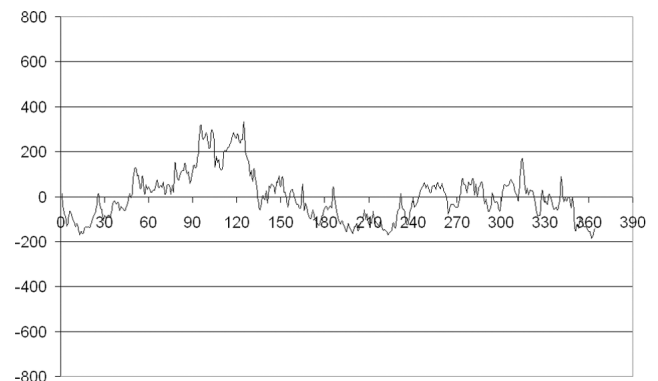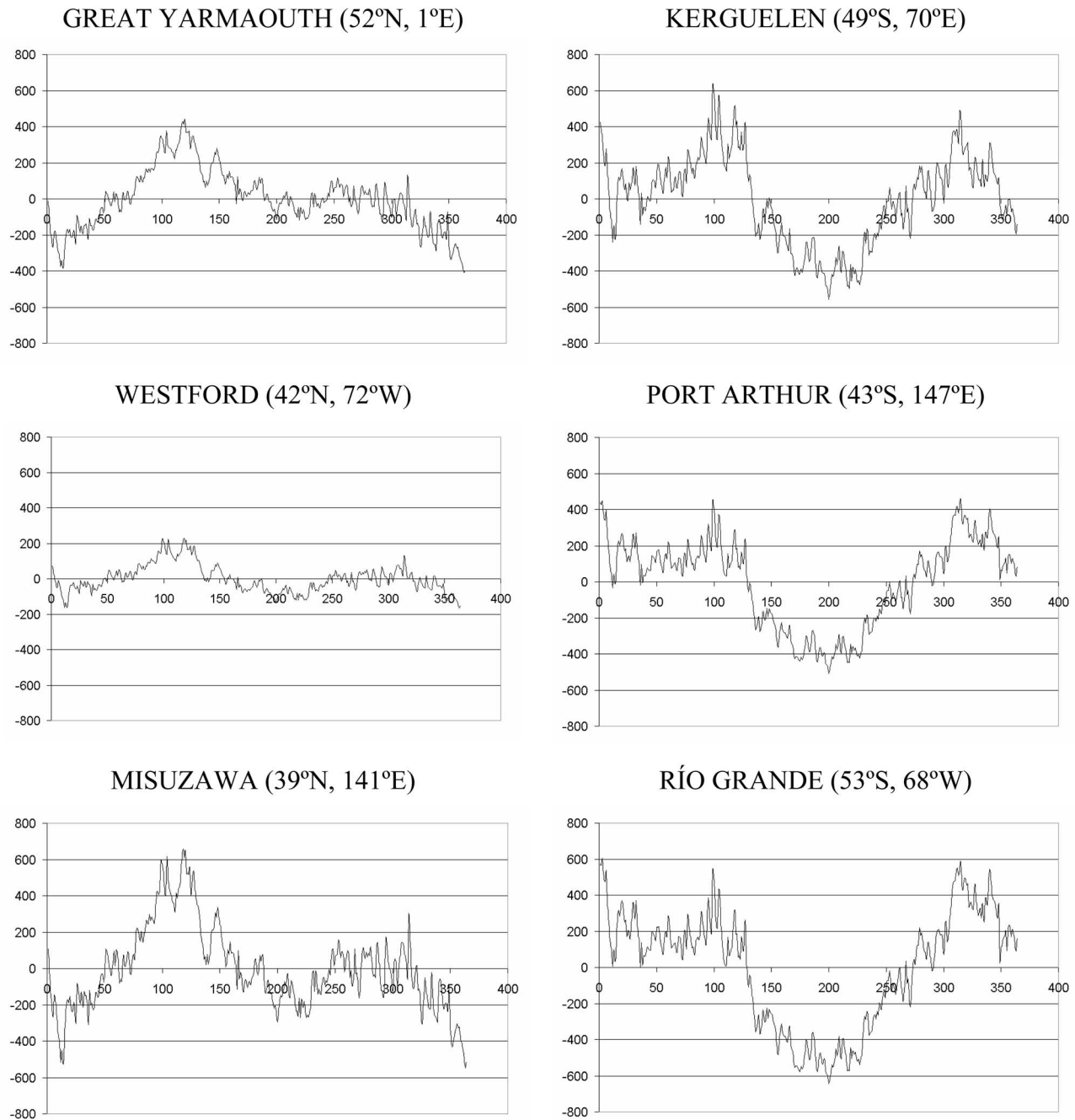

Figure 8. Time variation in the second mode for 1200 LT.

Figure 10. Time variation in the second mode for 2200 LT.

Local noon 12 p.m.

Figure 11. PCA analysis for different geomagnetic region at 1200 LT.

it is possible to see a component of the annual anomaly especially for low midlatitudes. Doing the same analysis for 2200 LT, similar results to *Zhao et al.* [2007] where found, highlighting a weak component of the annual anomaly.
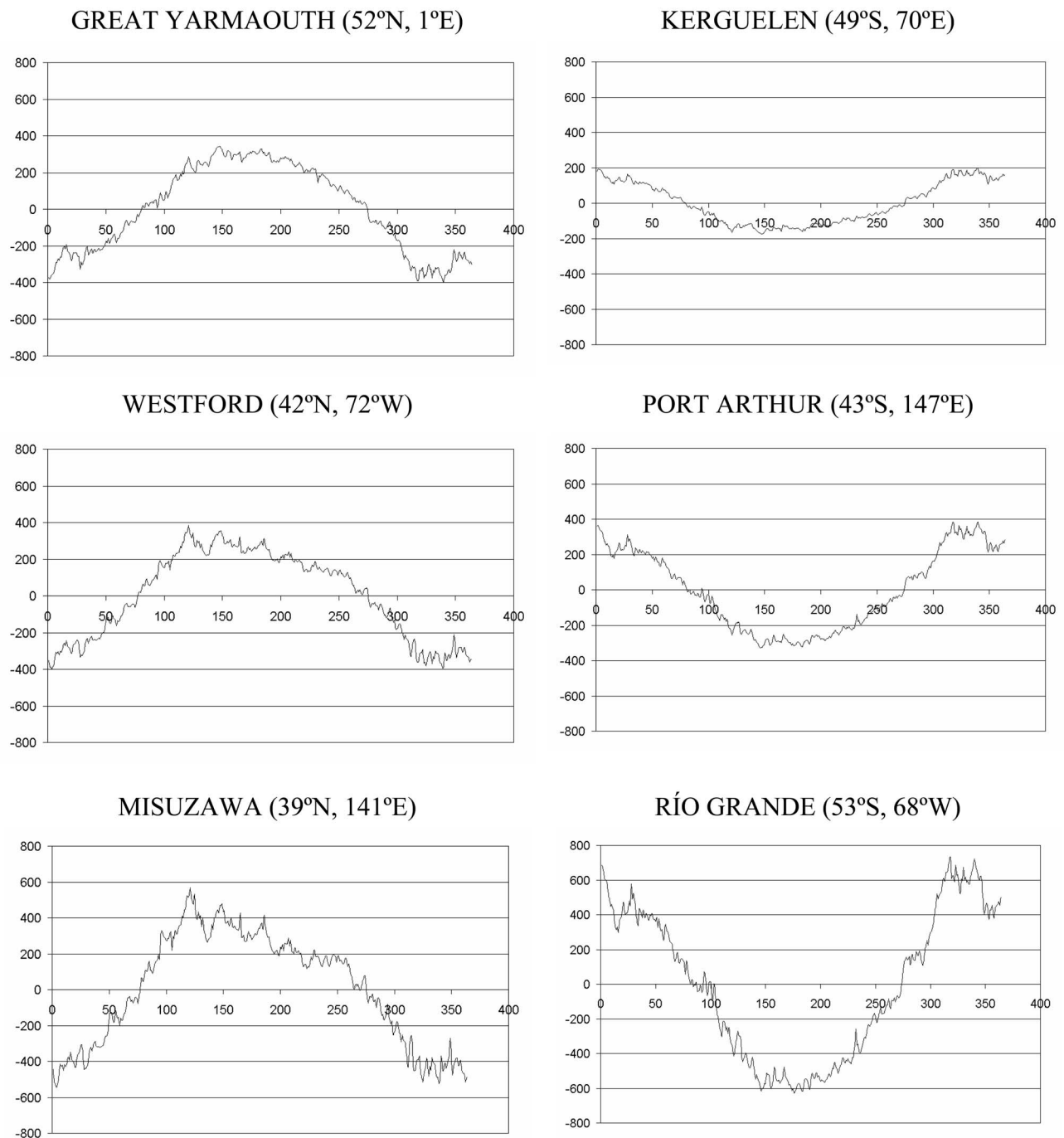
3.2. Fourier Analysis

[27] PCA results are compared with those obtained using Fourier analysis. So the amplitude of the first and second mode for 1200 LT and 2200 LT are analyzed using Fourier series. The equation used to fit is:

$$r(t, x) = A_{c1} \cos\left(\frac{t*2\pi}{1}\right) + A_{s1} \sin\left(\frac{t*2\pi}{1}\right) + A_{c2} \cos\left(\frac{t*2\pi}{0.5}\right)$$
$$+ A_{s2} \sin\left(\frac{t*2\pi}{0.5}\right) \qquad (11)$$

Local night 10 p.m.

Figure 12. PCA analysis for different geomagnetic region at 2200 LT.

where t is in year units and x represents the space (latitude and longitude). A_{C1}, A_{S1}, A_{C2}, and A_{S2} are the unknown Fourier series coefficients. This Fourier series is fitted for every latitude and longitude during the year 2006, allowing to carry out amplitude and initial phase for global representation.

3.2.1. Local Time: Noon

[28] Figure 15 shows the amplitude and phase of the annual and semiannual components obtained using equation (11).

Annual component: The amplitudes are significant at low latitudes and for midlatitudes in the Southern Hemisphere, showing maximal values near the south crest of the equatorial anomaly. The initial phase in the Southern Hemisphere is January for middle and high latitudes; while at low latitudes in the Northern and Southern hemispheres oscillate between February and March. We conclude that the behavior of the annual component presents maximal values between
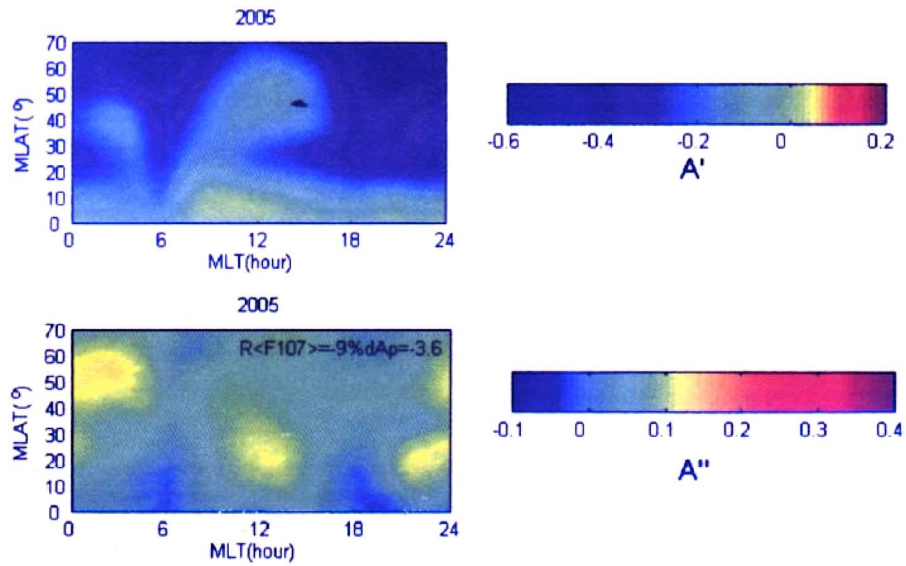
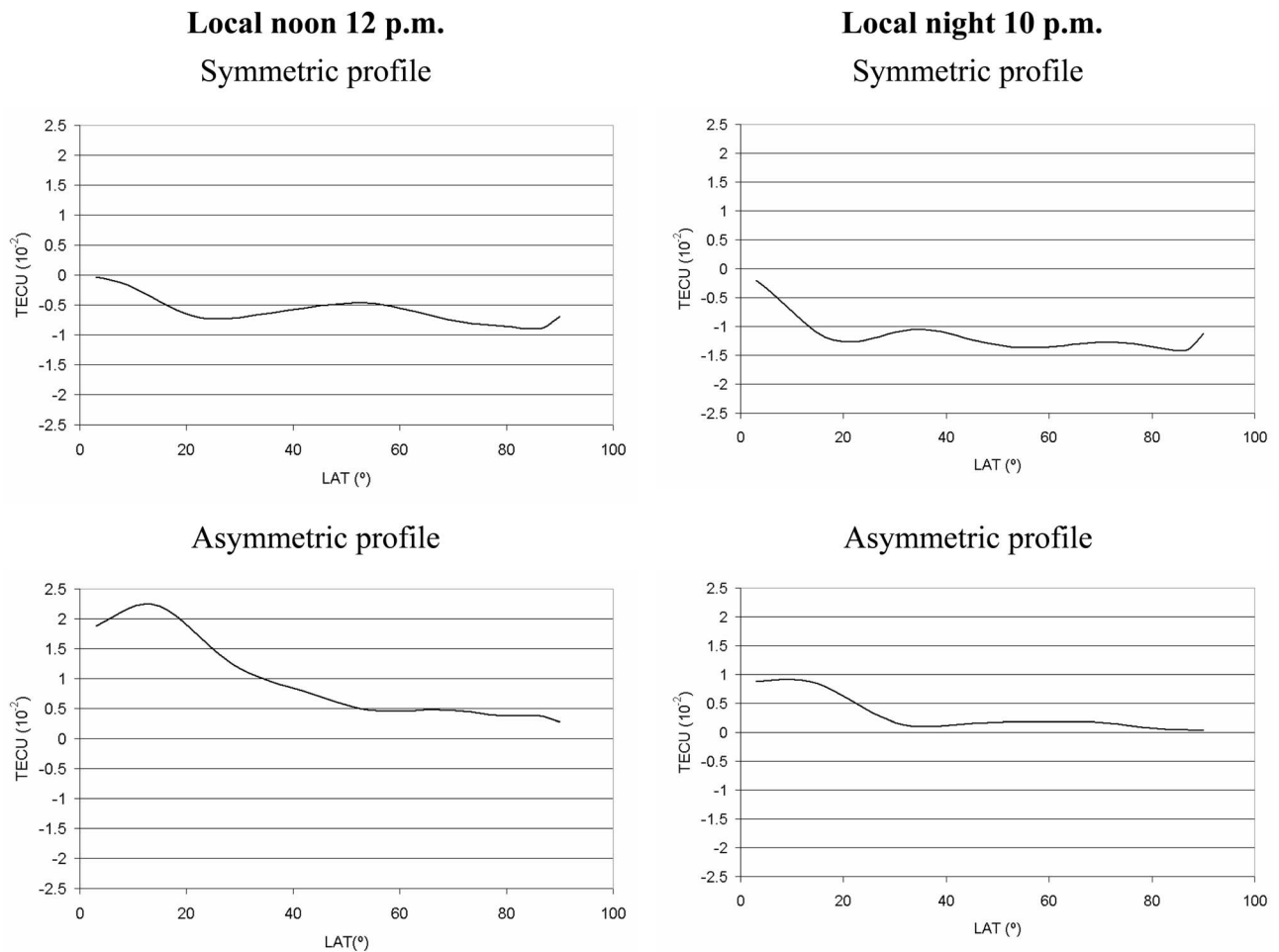**Figure 13.** Symmetric and asymmetric distribution by *Zhao et al.* [2007].
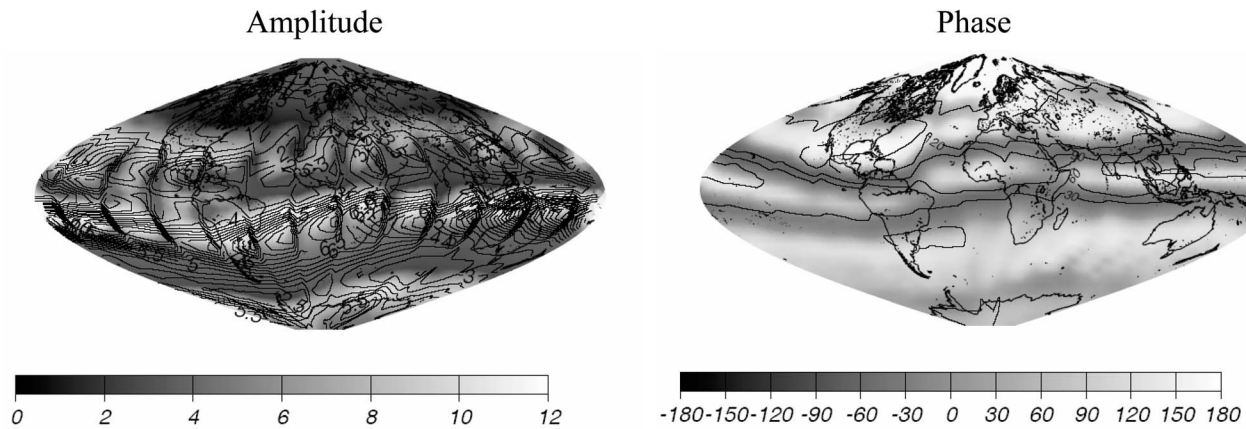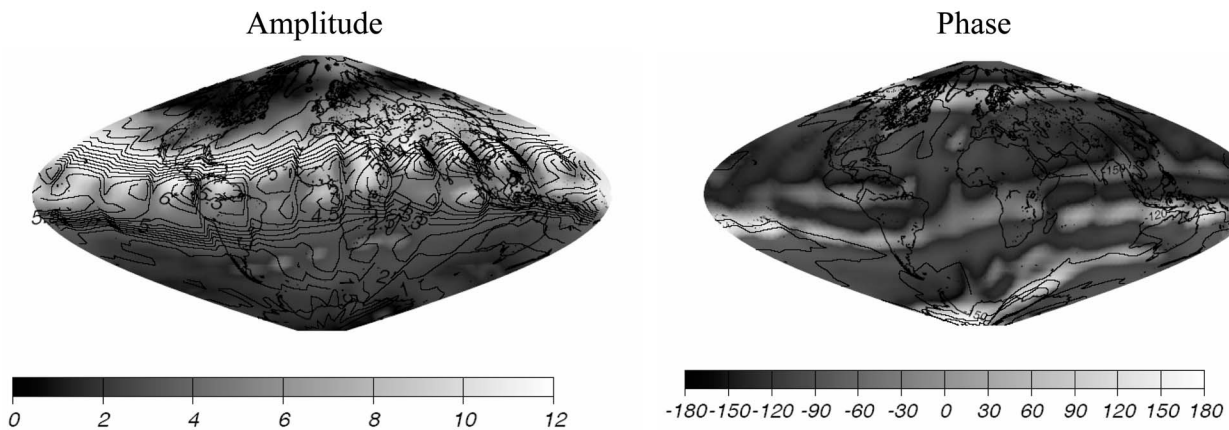
Local noon 12 p.m.

Symmetric profile

Local night 10 p.m.

Symmetric profile

Asymmetric profile

Asymmetric profile

Figure 14. Symmetric and asymmetric profiles of A_1 for 1200 LT and 2200 LT.

Local noon 12 p.m.

Annual Component

Amplitude

Phase

Semiannual Component

Amplitude

Phase

Figure 15. Amplitude and phase of the annual and semiannual component for local noon.

January and March. Semiannual component: The amplitudes are greater near to the geomagnetic equatorial regions and the initial phase is displaced to September–October.

3.2.2. Local Time: Night

[29] Figure 16 shows the amplitude and phase of the annual and semiannual components obtained using equation (11). Annual component: The amplitudes at low, middle, and high latitudes in the Southern Hemisphere are lower than at local 1200; for the Northern Hemisphere, the amplitudes are higher than at 1200 LT. The initial phase of the Southern Hemisphere is January; for the Northern Hemisphere, it is close to June–July. Semiannual component: The maximum variations of the amplitudes are near the equatorial region and their initial phase is close to October.

[30] To complete the comparison between both techniques we compare the size of the residuals after removing the first two modes. Table 1 shows for each technique both for 1200 LT and 2200 LT the portion of the original signal that remains unmodeled after using the first two modes: The first column shows the RMS value of the original signal and

the second column shows the RMS of the residuals after removing the first mode. The third column shows the RMS of the residuals after removing the first two modes.

[31] At noon, the portion of the original signal that remains unmodeled using only the first mode is 66% using PCA and 74% using Fourier analysis. After modeling with modes 1 and 2, 47% of the original signal remains unmodeled for PCA versus 58% in the case of Fourier analysis. At night, the differences are very small. For mode 1, PCA yields 66% of the original signal unmodeled while for Fourier we obtained 65%. For modes 1 and 2, the results are 50% and 52% for PCA and Fourier, respectively.

4. Conclusions

[32] The application of PCA on VTEC data is a useful technique to analyze the spatial and temporal variability of the ionosphere. In this work, it was possible to compound 78% of the variability contained in global GPS-derived VTEC data (for 2006) using only the first two modes. Both

Local night 10 p.m.

Annual Component

Amplitude   Phase
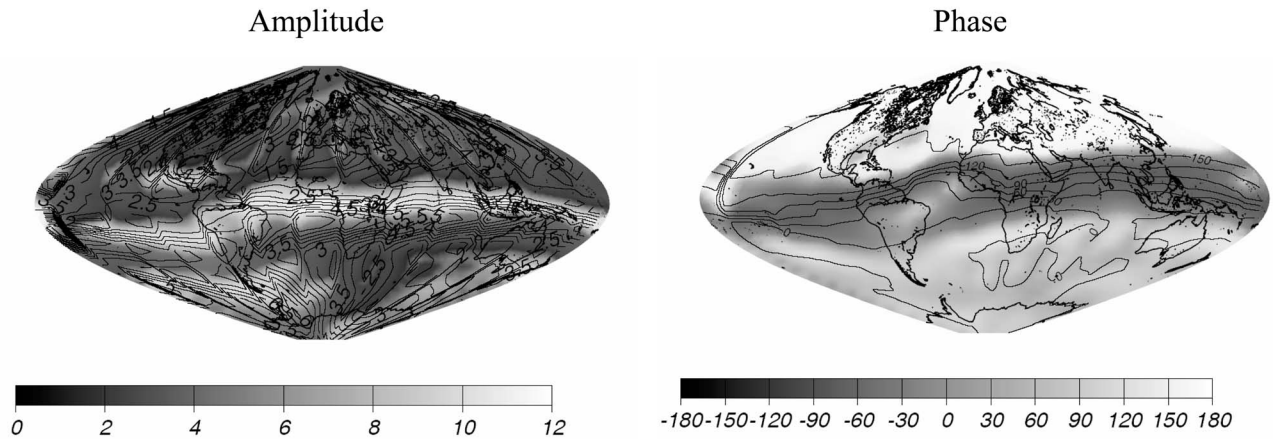
Semiannual Component
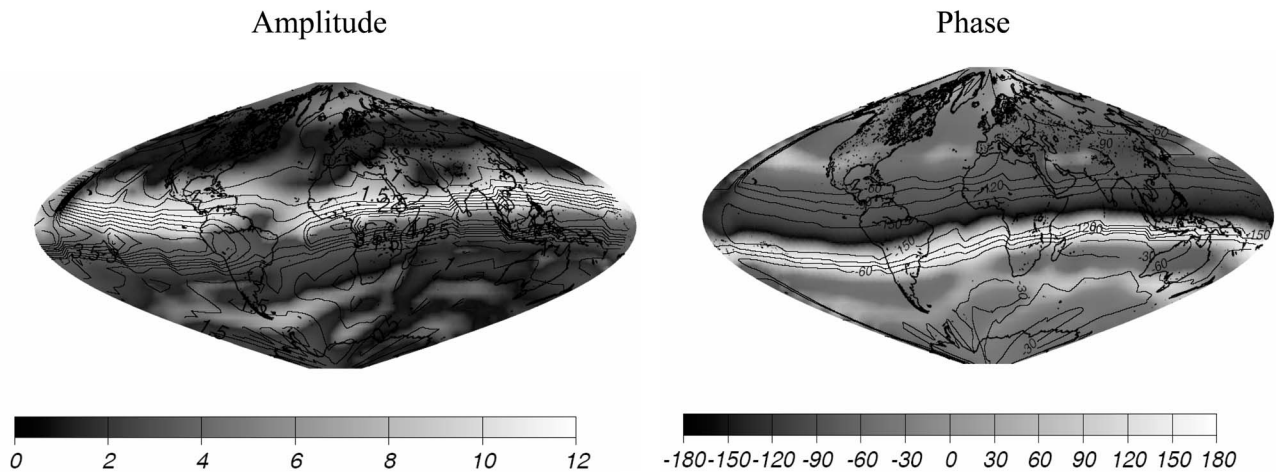
Amplitude   Phase

Figure 16. Amplitude and phase of the annual and semiannual component for local night.

the spatial distribution and the temporal variation are discussed for the first two modes. The main results are: (1) PCA technique combined with IGS VTEC global maps offers time and spatial representation of the ionospheric variation; and (2) PCA is based on orthogonal decomposition of the data itself without forcing an annual and a semiannual component as in Fourier analysis. For example, in the temporal variation it is possible to see a semiannual variability of mode 2 for 1200 with greatest peak on March equinox than on September one, while in Fourier analysis the semiannual component doesn't show this asymmetry.

[33] For Noon, the first and second modes have a significant contribution to the VTEC variance (they are a combination of the annual and semiannual variations). In the first mode, it is possible to see an annual component modulated by a semiannual one, resulting a variation with maximal values between October and February and minimal in June to July. In the second mode, a semiannual component was found, and the peak variation on the March–April equinox is higher than the September–October one.

[34] For night, the first mode shows a purely annual component. For mode 2, the semiannual component is modulated by an annual one, producing a higher March–April equinox peak than the September–October one.

[35] Comparing the results presented in this work with other authors that use classical Fourier series to represent the ionospheric variability, similar results were found. The amplitude and initial phase obtained using Fourier series show that the spatial and temporal variation behaviors are similar to the results obtained with PCA analysis. However,

Table 1. RMS of the Residuals After Removal of the First Two Modes

		PCA		Fourier Analysis	
Time	Original	Mode 1	Modes 1 + 2	Annual	Annual and Semiannual
1200 LT	4.48	2.96	2.11	3.34	2.62
2200 LT	3.51	2.31	1.76	2.28	1.84

PCA second mode clearly shows the asymmetry of the equinox peaks as was shown by *Zou et al.* [2000]. This effect is not evident from the Fourier analysis.

[36] For 1200 LT, it was shown that the PCA technique is more efficient to model the signal. For 2200 LT, PCA is only slightly better. This may be because the ionospheric variability during the night shows clearly dominant annual and semiannual components.

[37] Finally, further work needs to be carried out to investigate the VTEC variability during solar activity. The IGS VTEC global maps produced by IGS have been demonstrating a great utility to do this analysis.

References

Buonsanto, M. J. (1986), Possible effects of the changing Earth-Sun distance on the upper atmosphere, *South Pacific J. Nat. Sci.*, *8*, 58–65.

Chapman, S. (1931), The absorption and dissociatival or ionizing effect of monochromatic radiation in atmosphere on a rotating earth, *Proc. Phys. Soc.*, *43*, 483–501.

Feltens, J., and S. Schaer (1998), IGS products for the ionosphere, in *Proceedings of the IGS Analysis Center Workshop*, edited by J. M. Dow, J. Kouba, and T. Springer, pp. 225–232, Eur. Space Agency, Darmstadt, Germany.

Fuller-Rowell, T. J. (1998), The "thermospheric spoon": A mechanism for the semi-annual density variation. *J. Geophys. Res.*, *103*, 3951–3956.

Huang, Y. N., and K. Cheng (1996), Solar cycle variations of the equatorial ionospheric anomaly in total electron content in the Asian region, *J. Geophys. Res.*, *101*, 24,513–24,520.

Lal, C. (1992), Global F2 layer ionization and geomagnetic activity, *J. Geophys. Res.*, *97*, 12,153–12,159.

Lal, C. (1998), Solar wind and equinoctial maxima in geophysical phenomena, *J. Atmos. Sol. Terr. Phys.*, *60*, 1017–1024.

Meza, A., and M. P. Natali (2008), Annual and semiannual TEC effects at low solar activity in midlatitude Atlantic region based on TOPEX, *J. Geophys. Res.*, *113*, D14115, doi:10.1029/2007JD009088.

Nerem, R. S., E. J. Schrama, C. J. Koblinsky, and B. D. Beckley (1994), A preliminary evaluation of ocean topography from the TOPEX/POSEIDON mission, *J. Geophys. Res.*, *99*, 24,565–24,583.

Nerem, R. S., K. E. Rachlin, and B. D. Beckley (1997), Characterization of global mean sea level variations observed by TOPEX/POSEIDON using empirical orthogonal functions, *Surv. Geophys.*, *18*, 293–302.

Preisendorfer, R. W. (1988), *Principal Component Analysis in Meteorology and Oceanography*, 424 pp., Elsevier, Amsterdam.

Press, W. H., and B. P. Flannery (1995), *Numerical Recipes in FORTRAN 77: The Art of Scientific Computing (v. 1)*, 992 pp., Cambridge Univ. Press, Cambridge, U. K.

Rishbeth, H., and C. S. G. K. Setty (1961), The F-layer at sunrise, *J. Atmos. Sol. Terr. Phys.*, *21*, 263–276.

Schaer, S., G. Beutler, and M. Rothacher (1998), Mapping and predicting the ionosphere, paper presented at IGS AC Workshop, Darmstadt, Germany.

Torr, M. R., and D. G. Torr (1973), The seasonal behavior of the F2-layer of the ionosphere, *J. Atmos. Sol. Terr. Phys.*, *35*, 2237–2251.

Wu, C. C., C. D. Fryb, J. Y. Liu, K. Lioud, and C. L. Tseng (2004), Annual TEC variation in the equatorial anomaly region during the solar minimum: September 1996–August 1997, *J. Atmos. Sol. Terr. Phys.*, *66*, 199–207.

Zhao, B., W. Wan, L. Liu, X. Yue, and S. Venkatraman (2005), Statistical characteristics of the total density in the topside ionosphere during the period 1996–2004 using empirical orthogonal function (EOF) analysis, *Ann. Geophys.*, *23*, 3615–3631.

Zhao, B., W. Wan, L. Liu, T. Mao, Z. Ren, M. Wang, and A. B. Christensen (2007), Features of annual and semiannual variations derived form the global ionospheric maps of total electron content, *Ann. Geophys.*, *25*, 2513–2527.

Zou, L., H. Rishbeth, I. C. F. Müller-Wodarg, A. D. Aylward, G. H. Millward, T. J. Fuller-Rowell, D. W. Idenden, and R. J. Moffettt (2000), Annual and semiannual variations in the ionospheric F2-layer. I. Modelling, *Ann. Geophys.*, *18*, 927–944.

A. Meza and M. P. Natali, Facultad de Ciencias Astronómicas y Geofísicas, Universidad Nacional de La Plata, Paseo del Bosque s/n, 1900 La Plata, Argentina. (paula@fcaglp.unlp.edu.ar)